

Spontaneous decay of an emitter's excited state near a finite-length metallic carbon nanotube

A. M. Nemilentsau, G. Ya. Slepyan, and S. A. Maksimenko

Institute for Nuclear Problems, Belarus State University, Bobruiskaya 11, 220030 Minsk, Belarus

A. Lakhtakia

*Department of Engineering Science and Mechanics,
Pennsylvania State University, University Park, PA 16802, USA*

S. V. Rotkin

*Department of Physics, and Center for Advanced Materials and Nanotechnology,
Lehigh University, 16 Memorial Dr. E., Bethlehem, PA 18015, USA*

(Dated: Today)

The spontaneous decay of an excited state of an emitter placed in the vicinity of a metallic single-wall carbon nanotube (SWNT) was examined theoretically. The emitter-SWNT coupling strongly depends on the position of the emitter relative to the SWNT, the length of the SWNT, the dipole transition frequency and the orientation of the emitter. In the high-frequency regime, dips in the spectrum of the spontaneous decay rate exist at the resonance frequencies in the spectrum of the SWNT conductivity. In the intermediate-frequency regime, the SWNT conductivity is very low, and the spontaneous decay rate is practically unaffected by the SWNT. In the low-frequency regime, the spectrum of the spontaneous decay rate contains resonances at the antennas resonance frequencies for surface-wave propagation in the SWNT. Enhancement of both the total and radiative spontaneous decay rates by several orders in magnitude is predicted at these resonance frequencies. The strong emitter-field coupling is achieved, in spite of the low Q factor of the antenna resonances, due to the very high magnitude of the electromagnetic field in the near-field zone. The vacuum Rabi oscillations of the population of the excited emitter state are exhibited when the emitter is coupled to an antenna resonance of the SWNT.

PACS numbers: 78.67.Ch, 42.50.Nn, 33.70.Ca, 42.25.Fx

I. INTRODUCTION

The process of the spontaneous decay of an excited state of an emitter (atom, molecule, quantum dot, etc.) is strongly affected by the surroundings the emitter placed in. In fact, any non-homogeneity in the medium surrounding an emitter—including the very simple case of an interface of two different materials—will result in modification of the decay time (as well as the angular distribution of the radiated power) due to the interaction with the surface/interface modes [1, 2].

The physical scenario becomes especially interesting when the electromagnetic field (EMF) modes are quantized in a resonator, an open resonator or another photonic structure. Certain types of nanostructured resonators have a strongly inhomogeneous spatial or spectral distribution of the photonic density of states (DOS). The dynamics of an emitter coupled to such a resonator becomes non-Markovian [3–9]. Two relevant types of resonators or structured reservoirs are being studied these days: microcavities [3–5] and photonic crystals [6–8]. Among notable phenomena in the resonators are: (i) vacuum Rabi oscillations in the spontaneous decay of an atom coupled to a mode of a high-Q microcavity [4, 5], and (ii) complete freezing of the spontaneous decay process of an emitter with its transition frequency inside the band gap of a photonic crystal [7, 8].

Antenna-like structures furnish another example of an open resonator with a specific photonic DOS. One can

consider nanoantennas as structured photonic reservoirs of a new type, which should act similarly to microcavities and photonic crystals. Nanoantennas are also appealing as new tools for controlling emitter dynamics.

Nanoantennas of a particularly interesting type comprise nanoparticles made of plasmonic metals. For example, substantial enhancement of the fluorescence signal of an emitter placed in the vicinity of such nanoparticles [10–14] or nanoapertures [15] has been experimentally demonstrated. The spontaneous decay of quantum dots has been suggested [16, 17] to be an efficient way to generate optical plasmons in metallic nanowires to which the quantum dots are coupled. The crucial influence of antenna resonances in a gold nanodisk on the decay rate of a nearby quantum emitter has been theoretically predicted [18].

A single-wall carbon nanotube (SWNT) can function as a nanoantenna [19–25]. The cross-sectional diameter of a SWNT is of the order of a few nanometers while its length may be as large as several centimeters. The structural symmetry of the SWNT is denoted by a pair of indices (m, n) . A SWNT may exhibit either metallic/quasi-metallic properties (for $m - n = 3q$, where q is an integer) or semiconducting behavior ($m - n \neq 3q$) [26].

The propagation of the surface electromagnetic waves [27] along the surface of a SWNT determines its scattering and radiation characteristics [19, 20]. The antenna resonances of the surface waves in a SWNT are the origin of the pronounced peaks in the spectrum of its photonic

DOS [28] and, correspondingly, in the spectrum of thermal radiation if the SWNT is metallic [29]. These resonances can be also seen in the polarizability tensor and in the input impedance of a metallic SWNT. The resonance frequencies lie in the terahertz/infrared regime, depending on the SWNT length [19, 20]. These antenna resonances were shown to strongly affect the electromagnetic coupling between a SWNT and a plasmonic nanosphere [30] or a dipole [31]. Their effect on the spontaneous decay of a nearby emitter is reported here.

A strong enhancement of the spontaneous decay rate of an excited atomic state was theoretically predicted for an atom placed in close proximity of the surface of an infinitely long SWNT [32, 33], although antenna effects were neglected in these studies. We focus here on the combination of the antenna and near-field effects, and their influence on the process of the spontaneous decay of an emitter coupled to a SWNT nanoantenna. Besides a fundamental theoretical interest, practical applications can be foreseen, for example, in the fluorescence microscopy with SWNT-based probes [34, 35]. Moreover, the integration of SWNTs as nanoantennas with the nanoscale luminescent materials such as quantum dots [36–38] allows multifunctional nanostructures. Not only may these nanostructures exhibit biocompatibility and fluorescence, but also other characteristics useful for cancer diagnostics and therapeutics, as well as for drug storage and delivery.

In Sec. II we consider the decay dynamics of the emitter in the weak-coupling regime. The characteristics of the strong-coupling regime are discussed in Sec. III followed by conclusions in Sec. IV. Gaussian units are used throughout, an $\exp(-i\omega t)$ dependence on time is implicit, $\mathbf{e}_{x,y,z}$ are the unit Cartesian vectors, and all tensors are of the second order.

II. WEAK-COUPLING REGIME: SPONTANEOUS EMISSION

Let us consider the spontaneous decay of an excited state of an emitter placed in the vicinity of a SWNT of finite length L , as shown in Fig. 1. The emitter, located at \mathbf{r}_s , is modeled by a two-level system with transition frequency ω_e and dynamic electric dipole moment \mathbf{p}_0 . In the weak-coupling regime, the decay process is Markovian and the evolution of the excited state's occupation probability $|C_u(t)|^2$ is described by the exponential law [9, 32, 33]:

$$|C_u(t)|^2 = e^{-\Gamma_{cn}(\mathbf{r}_s, \omega_e)t}, \quad (1)$$

where

$$\begin{aligned} \Gamma_{cn}(\mathbf{r}_s, \omega_e) &= \frac{2\omega_e^2}{\hbar c^2} \mathbf{p}_0 \cdot \text{Im} \left[\underline{\underline{G}}(\mathbf{r}_s, \mathbf{r}_s, \omega_e) \right] \cdot \mathbf{p}_0 \\ &= \Gamma_0 \left\{ 1 + \frac{3c}{2\omega_e} \hat{\mathbf{p}}_0 \cdot \text{Im} \left[\underline{\underline{G}}^{(sc)}(\mathbf{r}_s, \mathbf{r}_s, \omega_e) \right] \cdot \hat{\mathbf{p}}_0 \right\} \quad (2) \end{aligned}$$

is the spontaneous decay rate, $\Gamma_0 = 4\omega_e^3 |\mathbf{p}_0|^2 / 3\hbar c^3$ is the free-space decay rate, $\hat{\mathbf{p}}_0$ is the unit vector along the di-

rection of polarization of the electric dipole, c is the speed of light in vacuum, \hbar is the reduced Plank's constant and the Green tensor $\underline{\underline{G}}(\mathbf{r}, \mathbf{r}'; \omega)$ is the solution of the Fredholm integral equation (A9). Equation (2) defines the total spontaneous decay rate of the emitter and includes both the radiative and the non-radiative decay rates.

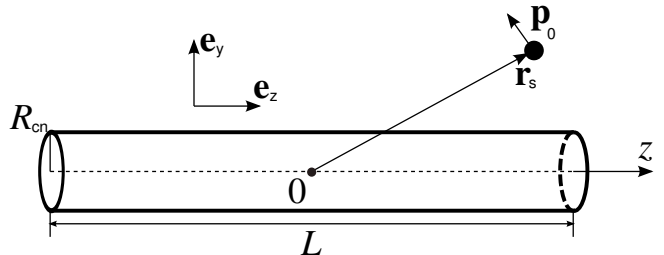


FIG. 1. Schematic representation of the emitter of electric dipole moment \mathbf{p}_0 located at \mathbf{r}_s in the vicinity of a SWNT of length L and cross-sectional radius R_{cn} . The origin 0 of the coordinate system lies at the centroid of the SWNT and the z axis is parallel to the axis of the SWNT.

The spectra of the normalized spontaneous decay rate Γ_{cn}/Γ_0 of an excited state of the emitter coupled to a metallic (15, 0) SWNT are presented in Fig. 2 for different locations and orientations of the emitter (Fig. 2a), different distances between the emitter and the SWNT (Fig. 2b), and different SWNT lengths (Fig. 2c). The spectra of the real and imaginary parts of the conductivity of the SWNT are presented in Fig. 2d. We can identify three regimes in the conductivity spectrum:

- (I) the high-frequency regime, $\omega_e/(2\pi) > 400$ THz, wherein the optical interband transitions dominate the SWNT conductivity;
- (II) the intermediate-frequency regime, $250 < \omega_e/(2\pi) < 400$ THz; and
- (III) the low-frequency regime, $\omega_e/(2\pi) < 250$ THz, wherein the conductivity follows the Drude model.

Let us consider first the high-frequency regime I in Fig. 2. The spontaneous decay rate demonstrates a significant dependence on the shortest distance d between the emitter and the closest point on the SWNT surface (Fig. 2b), thereby revealing the crucial influence of the near fields, as discussed later with reference to Fig. 3b.

The conductivity spectrum shows fixed resonances, identified by arrows in Fig. 2, that originate from the electron interband transitions between the Van Hove singularities in the electronic DOS. The spectra of the spontaneous decay rate of the emitter show dips at these frequencies. The frequencies of dips depend on the SWNT index (m, n) , but not on the length of the SWNT. Furthermore, the dip frequencies do not show any dependence on either the position or the orientation of the emitter. The magnitude of the spontaneous decay rate is affected by the orientation of the emitter (Fig. 2a) and is independent of L (Fig. 2c). Thus we conclude that these

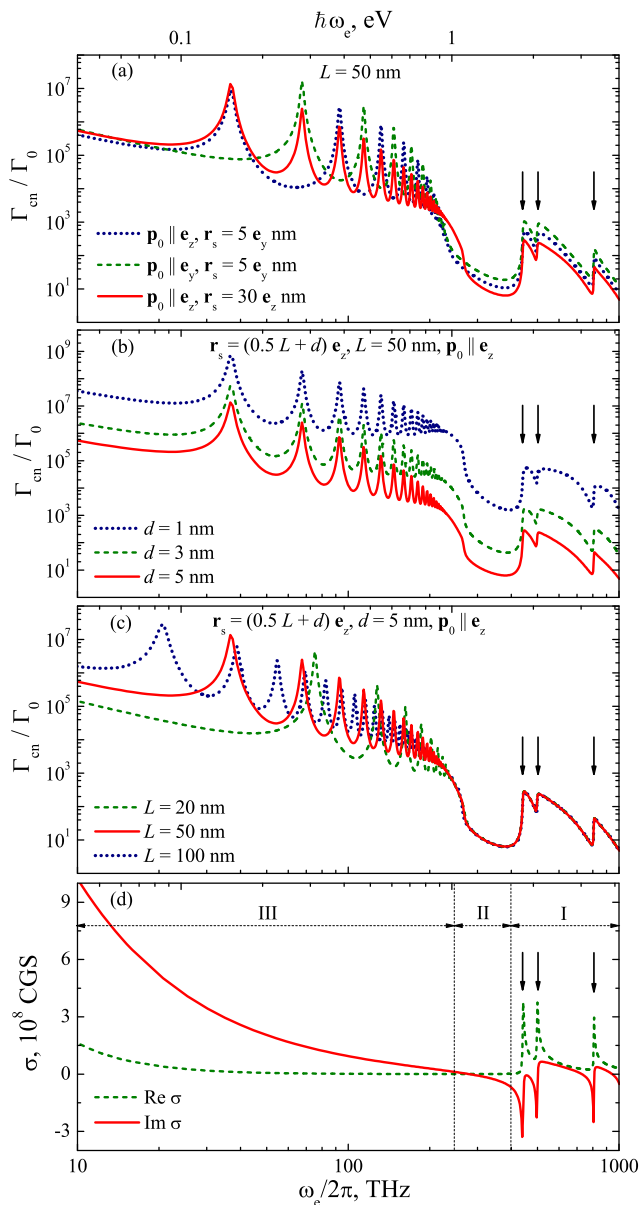


FIG. 2. Color online. (a)-(c) Normalized spontaneous decay rate Γ_{cn}/Γ_0 of an emitter coupled to a metallic (15,0) SWNT, as in Fig. 1, for (a) different positions \mathbf{r}_s and orientations $\mathbf{p}_0/|\mathbf{p}_0|$ of the emitter, assuming that the distance d between the emitter and the point on SWNT surface closest to the emitter remains the same; (b) different distances d ; (c) different lengths L of the SWNT. Equation (2) was used for calculating the decay rate. (d) Linear conductivity of the (15,0) metallic SWNT calculated using Eq. (36) in Ref. 27. The electronic relaxation time is assumed to be equal to 10^{-13} s.

near-field modes are not related to plasmonic resonances whose frequencies would scale with L .

In the intermediate-frequency regime II the conductivity of the SWNT is small and its antenna response is weak. Hence, the spontaneous decay rate is lower than

in the regimes I and III. Actually, the spontaneous decay rate is almost the same as the free-space decay rate (i.e., in the absence of the SWNT) when $d > 5$ nm. Our predictions for the decay dynamics in the frequency regimes I and II coincide with the results presented in Refs. 32 and 33 that were obtained for infinitely long SWNTs.

Most interesting is the low-frequency regime III, where the theoretical predictions made assuming the SWNT is infinitely long [32, 33] cannot explain the results. Particularly, Figs. 2a-c indicate the presence of several resonances instead of the monotonic decrease of the spontaneous decay rate with the decrease of the transition frequency of the emitter, as predicted in Refs. 32 and 33. The frequencies of these resonances coincide with the frequencies of the antenna resonances (arising from surface-wave propagation in the SWNT) defined by the space-quantization condition for plasmons [20]:

$$hL \approx \pi s, \quad (3)$$

where h is the guide wavenumber that is calculated using Eq. (58) of Ref. 27 and s is an integer. Furthermore, the location and the orientation of the emitter as well as the length of the SWNT strongly affect the spontaneous decay rate. In particular, only one type of resonances, with s being either odd for all resonances or even for all resonances, is present in the spectrum of the spontaneous decay rate if the emitter is located in the middle of the tube, *i.e.*, equidistant from both SWNT edges (Fig. 2a, $\mathbf{r}_s = 5\mathbf{e}_y$ nm). It depends on the orientation of the emitter with respect to the SWNT axis, which reflects odd or even symmetry of the dipole potential of the emitter. However, when the emitter is located on the SWNT axis, near one of the two edges of the SWNT and also oriented along the axis, both odd- s and even- s resonances are present. The symmetry in this case is full axial, although the mirror symmetry with respect the SWNT center is broken.

The spontaneous decay of the emitter strongly depends on the length of the SWNT. A decrease of L leads to the blue shift of the resonance frequencies (Fig. 2a), according to the space-quantization condition (3) for plasmons. Nevertheless, even for a short SWNT ($L \sim 20$ nm), at least a few resonances appear before the frequency regime II begins, where the resonances are not observable due to the strong attenuation of surface waves. Similar influence of the antenna resonances on the decay rate has been theoretically demonstrated for the case of an emitter coupled to a plasmonic (silver) nanodisk in Ref. 18.

Whereas Fig. 2 contains spectra of the normalized spontaneous decay rate Γ_{cn}/Γ_0 , the spectra of the actual spontaneous decay rate Γ_{cn} are interesting in their own right. Let us compare the spectrum of Γ_{cn} in Fig. 2 with the spectrum of Γ_{cn}/Γ_0 depicted as a solid line in Fig. 2b, both plots having been drawn for the same emitter-SWNT configuration. The off-resonance values of Γ_{cn} increase, but those of Γ_{cn}/Γ_0 decrease, as ω_e increases. Because $\Gamma_0 \propto \omega_e^3$ by definition, the off-resonance values of $\Gamma_{cn} \sim \omega_e^\alpha$, $\alpha \in (0, 3)$.

The dependence of Γ_{cn}/Γ_0 on the separation d between

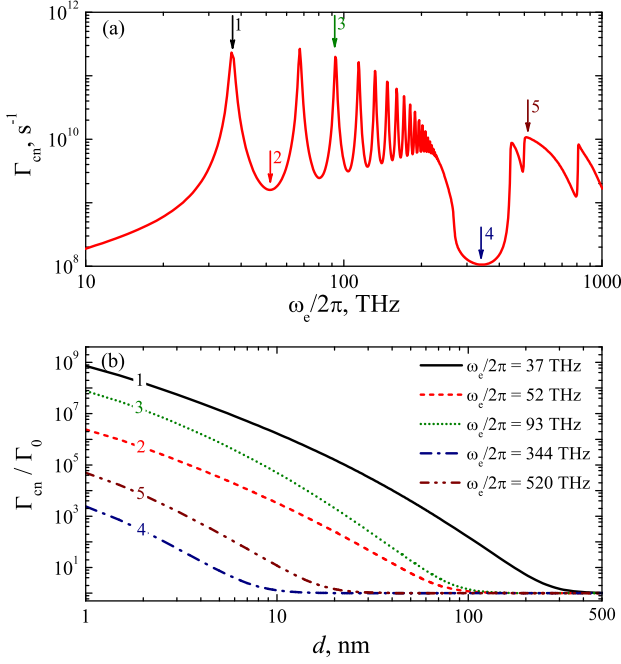


FIG. 3. Color online. (a) Spontaneous decay rate Γ_{cn} of an emitter with electric dipole moment $\mathbf{p}_0 = 1\mathbf{e}_z$ debye placed in the vicinity of an edge ($\mathbf{r}_s = 30\mathbf{e}_z$ nm) of a (15, 0) metallic SWNT of length $L = 50$ nm. The corresponding spectrum of the normalized decay rate Γ_{cn}/Γ_0 is presented as the solid line in Fig. 2b. (b) Dependence of Γ_{cn}/Γ_0 on the separation d between the SWNT edge and the emitter for different emitter frequencies indicated by arrows in Fig. 3a, when $\mathbf{r}_s = (L/2 + d)\mathbf{e}_z$ nm, $L = 50$ nm, and $\mathbf{p}_0 \parallel \mathbf{e}_z$.

the emitter and the nearest point on the SWNT surface is presented in Fig. 3b for five different values of ω_e identified in Fig. 3a. The enhancement indicated by $\Gamma_{cn}/\Gamma_0 > 1$ fades rapidly as d increases, which shows the crucial effect of the high magnitude of the electric field in the near-field zone. Let d_0 denote the value of d for which Γ_{cn} becomes equal to Γ_0 as d increases. Then, at the frequency of the first antenna resonance (curve labeled 1 in Fig. 3b), $d_0 \approx 0.1\pi c/\omega_e$; furthermore, d_0 decreases non-monotonically as ω_e increases. The values of d_0 at the antenna resonance frequencies of the SWNT are higher than the ones at the off-resonance frequencies. We also observe strong decrease of d_0 in the intermediate-frequency regime II.

The decay rate Γ_{cn} defined by Eq. (2) and depicted in Figs. 2 and 3 comprises a radiative part Γ_{rad} and a non-radiative part Γ_{nr} as follows:

$$\Gamma_{cn} = \Gamma_{rad} + \Gamma_{nr}. \quad (4)$$

The spontaneous radiative decay rate is given by [16, 39]:

$$\Gamma_{rad} = \eta\Gamma_{cn}, \quad (5)$$

where η is the radiation efficiency of the emitter in the presence of SWNT, as defined by Eq. (B1).

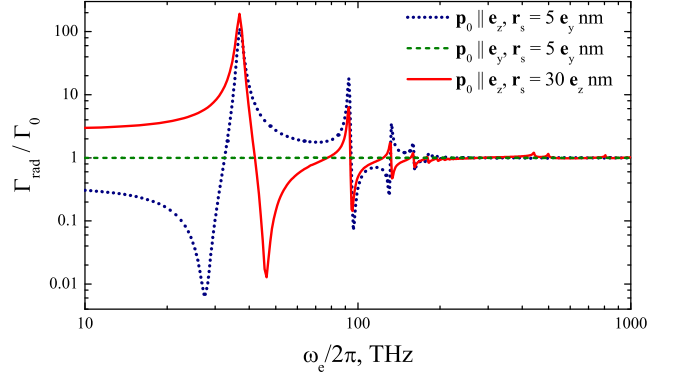


FIG. 4. Normalized spontaneous radiative decay rate Γ_{rad}/Γ_0 of the emitter coupled to a (15, 0) metallic SWNT for the same configurations as in Fig. 2a.

The spectra of Γ_{rad}/Γ_0 are presented in Fig. 4 for the same configurations as in Fig. 2a. Clearly, Γ_{rad} is enhanced much less than Γ_{cn} is. In fact, in the frequency regimes I and II we do not observe any enhancement of Γ_{rad} due to the presence of the SWNT.

In the frequency region III, resonances arise in the spectrum of Γ_{rad} provided the emitter is polarized parallel to the SWNT axis ($\mathbf{p}_0 \parallel \mathbf{e}_z$), the resonance frequencies being equal to the frequencies of antenna resonances defined by Eq. (3). The enhancement of the spontaneous radiative decay rate can be as high as 100 at the first resonance and falls rapidly as the resonance number s increases. When the emitter is placed near an edge of the SWNT, only odd- s resonances arise in the spectrum of Γ_{rad} , (solid line in Fig. 4), though both odd- s and even- s resonances are present in the spectrum of Γ_{cn} (solid line in Fig. 2a). The reason of the even- s resonances disappearance is the asymmetric distribution of the electric current induced in the SWNT by the emitter relative to the centroid of the SWNT that leads to the strong attenuation of the electromagnetic field radiated by the SWNT in the far-field zone. This is also the reason for the absence of resonances in the spectrum of Γ_{rad}/Γ_0 when the emitter is polarized normal to the SWNT axis (dashed line in Fig. 4).

In contrast to metallic SWNTs, the room-temperature conductivity of an intrinsic (undoped) semiconducting SWNT is low due to the low density of electrons in the conduction band. This leads to a strong attenuation of surface waves and, correspondingly, to the absence of resonances in the spectrum of the spontaneous decay rate as presented in Fig. 5. In the frequency regime I the contribution of the interband electron transitions dominates the SWNT conductivity. Then the spectrum of the spontaneous decay rate has similar features for both metallic and semiconducting SWNTs, *i.e.*, the dips are present at the resonance frequencies of the conductivity.

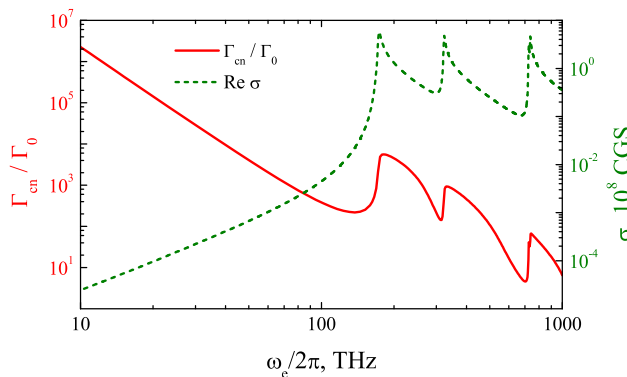


FIG. 5. Color online. Spontaneous decay rate of an emitter placed in the vicinity of a semiconducting (14,0) SWNT of length $L = 50$ nm; $\mathbf{p}_0 \parallel \mathbf{e}_z$ and $\mathbf{r}_s = 30\mathbf{e}_z$ nm.

III. STRONG-COUPLING REGIME: VACUUM RABI OSCILLATIONS

By virtue of Eq. (2) and the spectra of Γ_{cn}/Γ_0 presented in Fig. 2, we conclude that, in the presence of the (15,0) metallic SWNT, the spectra of the imaginary part of the diagonal elements of $\underline{\underline{G}}(\mathbf{r}_s, \mathbf{r}_s, \omega)$ must have pronounced resonances. So must the photonic DOS, as it is proportional to the trace of $\text{Im}\underline{\underline{G}}[(\mathbf{r}_s, \mathbf{r}_s, \omega)]$. Accordingly, a metallic SWNT can be considered as an open resonator (a structured reservoir) with a specific spectrum of quantized modes of the EMF. We suggest that the physics of an emitter coupled to these modes should be similar to the case of an emitter coupled to a microcavity [3] or a photonic crystal [7]: in particular, the Rabi oscillations of the population of the emitter's excited state are expected.

When the dipole transition frequency of the emitter, $\omega_e/2\pi$, is close to the frequency of a resonance of the photonic DOS, $\omega_\nu/2\pi$, a strong coupling develops between the field and the emitter. Assuming that the resonance in the photonic DOS spectrum can be approximated by a Lorentzian shape, we write:

$$\mathbf{p}_0 \cdot \text{Im} [\underline{\underline{G}}(\mathbf{r}, \mathbf{r}, \omega)] \cdot \mathbf{p}_0 = \frac{\mathbf{p}_0 \cdot \text{Im} [\underline{\underline{G}}(\mathbf{r}, \mathbf{r}, \omega_\nu)] \cdot \mathbf{p}_0 \gamma_\nu^2}{(\omega - \omega_\nu)^2 + \gamma_\nu^2}; \quad (6)$$

furthermore, we assume that the line width γ_ν is sufficiently small compared with the spectral separation between two adjacent resonance lines [9, Section 10.1.2]. Then the amplitude of the excited state is obtained as

$$C_u(t) = \frac{1}{\lambda_1 - \lambda_2} (-\lambda_2 e^{\lambda_1 t} + \lambda_1 e^{\lambda_2 t}), \quad (7)$$

where the temporal decay constants are

$$\lambda_{1,2} = \frac{1}{2}(i\delta_\nu - \gamma_\nu) \pm \frac{1}{2}\sqrt{(i\delta_\nu - \gamma_\nu)^2 - 2\Gamma(\mathbf{r}_s, \omega_e)\gamma_\nu} \quad (8)$$

and the detuning is $|\delta_\nu| = |\omega_e - \omega_\nu| \ll \omega_{e,\nu}$. For $\gamma_\nu \gg \Gamma(\mathbf{r}_s, \omega_e)$ we still get the exponential decay of an excited

state with decay rate $\Gamma(\mathbf{r}, \omega_e)$. However, for $2\Gamma(\mathbf{r}_s, \omega_e) > \gamma_\nu$ the Markovian approximation fails and the temporal evolution of the occupation probability amplitude of the excited state becomes non-monotonic.

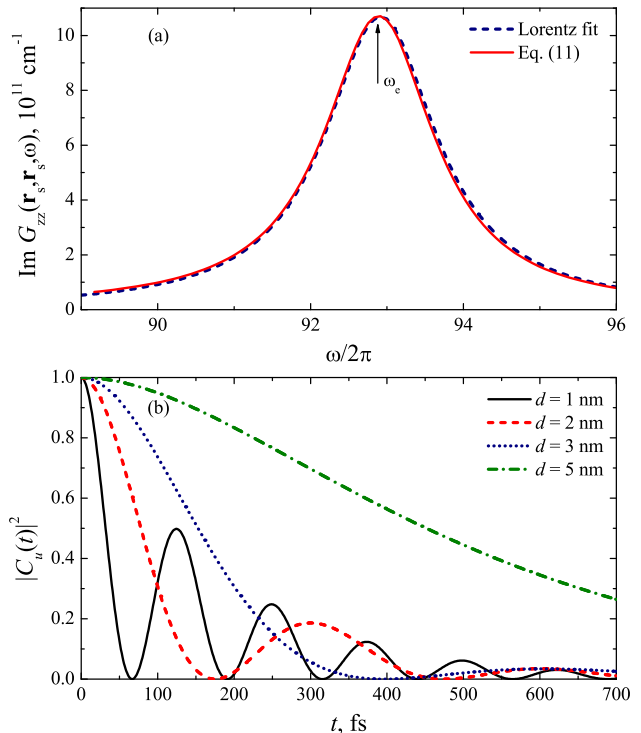


FIG. 6. Color online. (a) Solid line: $\mathbf{e}_z \cdot \text{Im} [\underline{\underline{G}}(\mathbf{r}_s, \mathbf{r}_s, \omega)] \cdot \mathbf{e}_z$ calculated using Eqs. (A6)–(A9) at $\mathbf{r}_s = 26\mathbf{e}_z$ nm near an edge of a (15,0) SWNT of length $L = 50$ nm. Dashed line: Lorentzian fit per Eq. (6) with $\omega_\nu = 5.84 \times 10^{14}$ rad/s and $\gamma_\nu = 5.6 \times 10^{12}$ rad/s. (b) The occupation probability $|C_u(t)|^2$ of an emitter excited state. The angular frequency ω_e of the dipole transition, designated by an arrow in Fig. 6a, is taken to be equal to ω_ν , i.e. $\delta_\nu = 0$. The transitional dipole moment of the emitter is $\mathbf{p}_0 = 10\mathbf{e}_z$ debye.

Let us consider the spontaneous decay of an emitter placed in the vicinity of a (15,0) metallic SWNT of length $L = 50$ nm and assume that the dipole transition frequency ω_e is close to the resonant frequency ω_ν . Figure 2 shows that the coupling of the emitter to the SWNT strongly depends on both the location and the orientation of the emitter in the low-frequency regime III. Suppose that $\mathbf{p}_0 = 10\mathbf{e}_z$ debye so that the emitter is oriented parallel to the SWNT axis, and that the emitter is placed close to one edge of the SWNT such that $\mathbf{r}_s = (L/2 + d)\mathbf{e}_z = 26\mathbf{e}_z$ nm. The spectrum of $\text{Im} [\mathbf{e}_z \cdot \underline{\underline{G}}(\mathbf{r}_s, \mathbf{r}_s, \omega) \cdot \mathbf{e}_z]$ at $\mathbf{r}_s = 26\mathbf{e}_z$ nm is presented in Fig. 6a near the resonance and is fitted by the Lorentzian function (6) with the parameters: $\omega_\nu = 5.84 \times 10^{14}$ rad/s and $\gamma_\nu = 5.6 \times 10^{12}$ rad/s. Even though the Q factor of this resonance is ~ 100 , which is much lower than in microcavities [5], we can still achieve a strong emitter-field coupling regime with an SWNT, due to the very high

magnitude of the EMF in the near-field zone.

The temporal evolution of the emitter excited state occupation probability is presented in Fig. 6b for different emitter-SWNT separations d , assuming that the detuning δ_ν is null-valued. For small emitter-SWNT separation distances ($d < 3$ nm), $C_u(t)$ provides an evidence of damped Rabi oscillations. The oscillation frequency decreases as the separation distance increases. Finally, for $d > 5$ nm, the spontaneous decay state becomes almost exponential. Thus, the strong emitter-field coupling can be detected for an emitter in the vicinity of a metallic SWNT acting as a resonator, although the coupling strength crucially depends on the emitter-SWNT separation. The coupling strength can be increased by using shorter SWNTs, as the blue-shift of the antenna resonance frequency leads to an increase in the Q factor.

IV. DISCUSSION AND CONCLUSION

Using the standard procedure of electromagnetic-field quantization in an absorbing medium [9, 32, 33], we theoretically studied the process of spontaneous decay of an excited state of an emitter placed in the vicinity of a metallic single-wall carbon nanotube. We demonstrated that a metallic SWNT can act as an open resonator (a structured reservoir) with a special density of quantized modes of the EMF in its vicinity. The emitter-SWNT coupling strongly depends on the position and the orientation of the emitter relative to the SWNT, the length of the SWNT, and the dipole transition frequency.

Three different frequency regimes were identified, based on the characteristics of the emitter-SWNT coupling. In the high-frequency regime, where the dominant contribution to the SWNT conductivity is due to the interband electron transitions, dips in the spectrum of the spontaneous decay rate (Fig. 2) exist at the resonance frequencies of the interband transition. The spontaneous decay rate of an excited state of the emitter is hardly influenced by the length of the SWNT in this regime, although it does depend on the location and the orientation of the emitter. In the intermediate-frequency regime, the SWNT conductivity is low, and the spontaneous decay rate is practically unaffected by the SWNT.

In the low-frequency regime, the intraband motion of electrons dominates the SWNT conductivity. The spectrum of the spontaneous decay rate shows resonances coinciding with the antenna resonance frequencies for electromagnetic waves (plasmons), propagating on the SWNT surface. Enhancement of the spontaneous decay rate by at least 7 orders in magnitude is predicted at the resonance frequencies (Fig. 2).

The contribution of the radiative decay to the spontaneous decay was estimated. The enhancement of the

spontaneous radiative decay rate by up to two orders of magnitude was demonstrated for an emitter polarized along the SWNT axis. The spontaneous radiative decay rate was not enhanced when the emitter is polarized normal to the SWNT axis.

When the emitter is placed several nanometers from the SWNT surface and the dipole transition frequency of the emitter is in the vicinity of an antenna resonance frequency of the SWNT, the emitter decay dynamics becomes non-Markovian. In particular, we clearly demonstrated vacuum Rabi oscillations (Fig. 6). The strong emitter-field coupling is achieved, in spite of the relatively low Q factor of the antenna resonances, due to the very high magnitude of the electromagnetic field in the near-field zone. Consequently, unlike a microcavity reservoir whose resonances have high Q factors, a metallic SWNT nanoantenna should radiate quite readily.

ACKNOWLEDGMENTS

This research was partially supported by (i) the Belarus Republican Foundation for Fundamental Research (BRFFR) under projects F10R-004 and F10Mld-003; (ii) EU FP7 under projects FP7-230778 TERACAN, FP7-247007 CACOMEL and FP7-266529 BY-NanoERA; and (iii) the Binder Endowment at the Pennsylvania State University.

Appendix A: Green tensor

The Green tensor $\underline{\underline{G}}(\mathbf{r}, \mathbf{r}_s, \omega)$ in Eq. (2) is the solution of the differential equation

$$[(\nabla_{\mathbf{r}} \times \underline{\underline{I}}) \cdot (\nabla_{\mathbf{r}} \times \underline{\underline{I}}) - k^2 \underline{\underline{I}}] \cdot \underline{\underline{G}}(\mathbf{r}, \mathbf{r}_s, \omega) = 4\pi \underline{\underline{I}} \delta(\mathbf{r} - \mathbf{r}_s) \quad (\text{A1})$$

which also satisfies jump conditions appropriate for the EMF across the SWNT surface as well as the Sommerfeld radiation conditions; here, $\underline{\underline{I}}$ is the identity tensor, $\delta(\cdot)$ is the Dirac delta function, and $k = \omega/c$ is free-space wavenumber.

Defining the vector field $\mathbf{G}^{(\beta)}(\mathbf{r}, \mathbf{r}_s, \omega) = \underline{\underline{G}}(\mathbf{r}, \mathbf{r}_s, \omega) \cdot \mathbf{e}_\beta$, ($\beta = x, y, z$), we write:

$$[(\nabla_{\mathbf{r}} \times \underline{\underline{I}}) \cdot (\nabla_{\mathbf{r}} \times \underline{\underline{I}}) - k^2 \underline{\underline{I}}] \cdot \mathbf{G}^{(\beta)}(\mathbf{r}, \mathbf{r}_s, \omega) = 4\pi \mathbf{e}_\beta \delta(\mathbf{r} - \mathbf{r}_s). \quad (\text{A2})$$

Thus, we can formally consider each column of the Green tensor $\underline{\underline{G}}(\mathbf{r}, \mathbf{r}_s, \omega)$ as a vector field $\mathbf{G}^{(\beta)}(\mathbf{r}, \mathbf{r}_s, \omega)$ induced at \mathbf{r} by a source current density located at \mathbf{r}_s and polarized parallel to the unit vector \mathbf{e}_β . Identifying the electric field $\mathbf{E}(\mathbf{r})$ as $\mathbf{G}^{(\beta)}(\mathbf{r}, \mathbf{r}_s, \omega)$ and the magnetic field $\mathbf{H}(\mathbf{r})$ as $(ik)^{-1} \nabla_{\mathbf{r}} \times \mathbf{G}^{(\beta)}(\mathbf{r}, \mathbf{r}_s, \omega)$, we see that $\mathbf{G}^{(\beta)}(\mathbf{r}, \mathbf{r}_s, \omega)$ satisfies two jump conditions across the SWNT surface [27]; thus,

$$\lim_{\delta \rightarrow 0} \left\{ \mathbf{u}_n \times \nabla \times \left[\mathbf{G}^{(\beta)}(\mathbf{r}_{cn} + \delta \mathbf{u}_n, \mathbf{r}_s, \omega) - \mathbf{G}^{(\beta)}(\mathbf{r}_{cn} - \delta \mathbf{u}_n, \mathbf{r}_s, \omega) \right] \right\} = \frac{4\pi ik^2}{\omega} \mathbf{j}^{(\beta)}(z, \mathbf{r}_s), \quad (\text{A3})$$

$$\lim_{\delta \rightarrow 0} \left\{ \mathbf{u}_n \times \left[\mathbf{G}^{(\beta)}(\mathbf{r}_{cn} + \delta \mathbf{u}_n, \mathbf{r}_s, \omega) - \mathbf{G}^{(\beta)}(\mathbf{r}_{cn} - \delta \mathbf{u}_n, \mathbf{r}_s, \omega) \right] \right\} = \mathbf{0}, \quad (\text{A4})$$

where

$$\left. \begin{aligned} \mathbf{r}_{cn} &= R_{cn} \mathbf{u}_n + z \mathbf{e}_z \\ \mathbf{u}_n &= \cos \phi \mathbf{e}_x + \sin \phi \mathbf{e}_y \end{aligned} \right\}, \quad (\text{A5})$$

the surface current density $\mathbf{j}^{(\beta)}(z, \mathbf{r}_s, \omega) = \mathbf{e}_z j^{(\beta)}(z, \mathbf{r}_s, \omega) = \sigma_{zz} \mathbf{e}_z \mathbf{e}_z \cdot \mathbf{G}^{(\beta)}(\mathbf{r}_{cn}, \mathbf{r}_s, \omega)$ is induced on the SWNT surface by the electric field $\mathbf{G}^{(\beta)}(\mathbf{r}_{cn}, \mathbf{r}_s)$, and σ_{zz} is the axial SWNT conductivity [27]. We impose the restriction $kR_{cn} \ll 2\pi$ to ensure that $j^{(\beta)}(z, \mathbf{r}_s, \omega)$ is uniform along the SWNT circumference.

So, the calculation of the Green tensor $\underline{\underline{G}}(\mathbf{r}, \mathbf{r}_s, \omega)$ requires us to solve three scattering problems. Each problem involves the scattering by the SWNT of the field radiated by an electric dipole, being oriented along one of the Cartesian axes. We have shown elsewhere [31] that such a boundary-value problem can be reduced to a Fredholm integral equation of the first kind for the current density

$j^{(\beta)}(z, \mathbf{r}_s, \omega)$. Thus, we decompose

$$\underline{\underline{G}}(\mathbf{r}, \mathbf{r}_s, \omega) = \underline{\underline{G}}^{(0)}(\mathbf{r}, \mathbf{r}_s, \omega) + \underline{\underline{G}}^{(sc)}(\mathbf{r}, \mathbf{r}_s, \omega), \quad (\text{A6})$$

where

$$\underline{\underline{G}}^{(0)}(\mathbf{r}, \mathbf{r}_s, \omega) = \left(\underline{\underline{I}} + \frac{\nabla \nabla}{k^2} \right) \frac{\exp(ik|\mathbf{r} - \mathbf{r}_s|)}{|\mathbf{r} - \mathbf{r}_s|} \quad (\text{A7})$$

is the free-space Green tensor and

$$G_{\alpha\beta}^{(sc)}(\mathbf{r}, \mathbf{r}_s, \omega) = \mathbf{e}_\alpha \cdot \underline{\underline{G}}^{(sc)}(\mathbf{r}, \mathbf{r}_s, \omega) \cdot \mathbf{e}_\beta = \frac{ik^2 R_{cn}}{\omega} \int_{-L/2}^{L/2} j^{(\beta)}(z, \mathbf{r}_s, \omega) \int_0^{2\pi} G_{\alpha z}^{(0)}(\mathbf{r}, \mathbf{r}_{cn}, \omega) d\phi dz, \quad (\text{A8})$$

represents the modification of the free-space Green tensor due to the presence of the SWNT. The integral equation for $j^{(\beta)}(z, \mathbf{r}_s, \omega)$ is

$$\int_{-L/2}^{L/2} j^{(\beta)}(z', \mathbf{r}_s, \omega) \mathcal{K}(z - z') dz' + C_1 e^{-ikz} + C_2 e^{ikz} = \frac{1}{2\pi} \int_{-L/2}^{L/2} \frac{e^{ik|z-z'|}}{2ik} \int_0^{2\pi} G_{z\beta}^{(0)}(\mathbf{r}'_{cn}, \mathbf{r}_s, \omega) d\phi' dz', \quad (\text{A9})$$

where C_1 and C_2 are constants to be determined from the edge conditions $j^{(\beta)}(\pm L/2, \mathbf{r}_s, \omega) = 0$. The kernel is

$$\mathcal{K}(z) = \frac{\exp(ik|z|)}{2ik\sigma_{zz}(\omega)} - \frac{2iR_{cn}}{\omega} \int_0^\pi \frac{e^{ikr}}{r} d\phi, \quad (\text{A10})$$

and $r = \sqrt{z^2 + 4R_{cn}^2 \sin^2(\phi/2)}$. This integral equation is numerically solvable [20, 29, 31].

Appendix B: Radiation efficiency

According to Chap. 8 of Ref. 39, in the weak emitter-field coupling regime we can consider an emitter as a classically oscillating at angular frequency ω_e . The radiation efficiency η of the emitter in the presence of an SWNT is defined as

$$\eta = \frac{P_{\text{rad}}}{P_{\text{rad}} + P_{\text{nr}}}, \quad (\text{B1})$$

where P_{rad} is the power radiated jointly by the emitter and the SWNT in the far-field zone and P_{nr} is the power

absorbed by the SWNT. In order to calculate P_{rad} and P_{nr} , we need to solve the problem of the scattering by the SWNT of the EMF radiated by the emitter. The electric field is the solution of Eq. (A2) with \mathbf{e}_β on the right side of the equation replaced by $k^2 \mathbf{p}_0$. It also has to satisfy the boundary conditions (A3) and (A4) on the SWNT surface. This problem has been studied in detail in our previous paper [31] and here we present only the main results.

The electric current $\mathbf{J}^{eq}(z) = J^{eq}(z) \mathbf{e}_z$ induced on the SWNT surface by the emitter is the solution of integral equation (A9) with $G_{z\beta}^{(0)}(\mathbf{r}'_{cn}, \mathbf{r}_s, \omega)$ on the right side of the equation replaced by $k^2 \mathbf{e}_z \cdot \underline{\underline{G}}^{(0)}(\mathbf{r}'_{cn}, \mathbf{r}_s, \omega) \cdot \mathbf{p}_0$. After finding $J^{eq}(z)$, the calculations of P_{rad} and P_{nr} are straightforward. Thus,

$$P_{\text{nr}} = \pi R_{cn} \text{Re} \left[\frac{1}{\sigma_{zz}} \int_{-L/2}^{L/2} |J^{eq}(z)|^2 dz \right] \quad (\text{B2})$$

and, with reference to a spherical coordinate system with origin at the centroid of the SWNT and $\mathbf{e}_{r,\theta,\phi}$ as its unit vector,

$$P_{\text{rad}} = \frac{cr^2}{8\pi} \int_0^\pi d\theta \sin\theta \int_0^{2\pi} d\phi \mathbf{e}_r \cdot \text{Re} \left\{ \frac{i}{k} \mathbf{E}_{\text{far}}(\mathbf{r}) \times [\nabla \times \mathbf{E}_{\text{far}}(\mathbf{r})]^* \right\}, \quad (\text{B3})$$

where the electric field in the far-field zone ($kr \gg 1$) is given by

$$\mathbf{E}_{\text{far}}(\mathbf{r}) \simeq \frac{e^{ikr}}{r} \left[k^2 e^{-ik\mathbf{e}_r \cdot \mathbf{r}_s} (\mathbf{e}_\theta \mathbf{e}_\theta + \mathbf{e}_\phi \mathbf{e}_\phi) \cdot \mathbf{p}_0 - \mathbf{e}_\theta \frac{i2\pi R_{cn}\omega \sin\theta}{c^2} \int_{-0.5L}^{0.5L} e^{-ikz \cos\theta} J^{eq}(z) dz \right]. \quad (\text{B4})$$

-
- [1] E. M. Purcell, Phys. Rev. **69**, 681 (1946).
[2] N. F. Shul'ga and V. V. Syshchenko, J. Phys.: Conf. Ser. **236**, 012010 (2010).
[3] B. J. Dalton, S. M. Barnett, and B. M. Garraway, Phys. Rev. A **64**, 053813 (2001).
[4] H. Walther, B. T. H. Varcoe, B.-G. Englert, and T. Becker, Rep. Prog. Phys. **69**, 1325 (2006).
[5] A. V. Kavokin, J. J. Baumberg, G. Malpuech, and F. P. Laussy, *Microcavities* (Oxford University Press, 2007).
[6] E. P. Petrov, V. N. Bogomolov, I. I. Kalosha, and S. V. Gaponenko, Phys. Rev. Lett. **81**, 77 (1998).
[7] P. Lambropoulos, G. M. Nikolopoulos, T. R. Nielsen, and S. Bay, Rep. Prog. Phys. **63**, 455 (2000).
[8] D. Mogilevtsev and S. Kilin, in *Progress in Optics 54*, edited by E. Wolf (Elsevier, New York, 2009), p. 89.
[9] W. Vogel and D.-G. Welsch, *Quantum Optics* (Wiley-VCH, 2006).
[10] P. Anger, P. Bharadwaj, and L. Novotny, Phys. Rev. Lett. **96**, 113002 (2006).
[11] P. Bharadwaj and L. Novotny, Opt. Express **15**, 14266 (2007).
[12] S. Kühn, G. Mori, M. Agio, and V. Sandoghdar, Mol. Phys. **106**, 893 (2008).
[13] H. Eghlidi, K. G. Lee, X.-W. Chen, S. Gotzinger, and V. Sandoghdar, Nano Lett. **9**, 4007 (2009).
[14] A. Mohammadi, F. Kaminski, V. Sandoghdar, and M. Agio, J. Phys. Chem. C **114**, 7372 (2010).
[15] D. Gérard, J. Wenger, N. Bonod, E. Popov, H. Rigneault, F. Mahdavi, S. Blair, J. Dintinger, and T. W. Ebbesen, Phys. Rev. B **77**, 045413 (2008).
[16] D. E. Chang, A. S. Sørensen, P. R. Hemmer, and M. D. Lukin, Phys. Rev. Lett. **97**, 053002 (2006).
[17] A. V. Akimov, A. Mukherjee, C. L. Yu, D. E. Chang, A. S. Zibrov, P. R. Hemmer, H. Park, and M. D. Lukin, Nature **450**, 402 (2007).
[18] R. Esteban, T. V. Teperik, and J. J. Greffet, Phys. Rev. Lett. **104**, 026802 (2010).
[19] G. W. Hanson, IEEE Trans. Antennas Propagat. **53**, 3426 (2005).
[20] G. Ya. Slepyan, M. V. Shuba, S. A. Maksimenko, and A. Lakhtakia, Phys. Rev. B **73**, 195416 (2006).
[21] P. J. Burke, S. Li, and Z. Yu, IEEE Trans. Nanotechnol. **5**, 314 (2006).
[22] J. Hao and G. W. Hanson, Phys. Rev. B **75**, 165416 (2007).
[23] G. Miano and F. Villone, IEEE Trans. Antennas Propagat. **54**, 2713 (2007).
[24] M. V. Shuba, S. A. Maksimenko, and A. Lakhtakia, Phys. Rev. B **76**, 155407 (2007).
[25] M. V. Shuba, G. Ya. Slepyan, S. A. Maksimenko, C. Thomsen, and A. Lakhtakia, Phys. Rev. B **79**, 155403 (2009).
[26] J.-Ch. Charlier, X. Blase, S. Roche, Rev. Mod. Phys. **79**, 677 (2007).
[27] G. Ya. Slepyan, S. A. Maksimenko, A. Lakhtakia, O. Yevtushenko, and A. V. Gusakov, Phys. Rev. B **60**, 17136 (1999).
[28] A. Nemilentsau, G. Ya. Slepyan, and S. A. Maksimenko, Phys. Scr. **T135**, 014041 (2009).
[29] A. M. Nemilentsau, G. Ya. Slepyan, and S. A. Maksimenko, Phys. Rev. Lett. **99**, 147403 (2007).
[30] G. W. Hanson, IEEE Trans. Antennas Propagat. **55**, 3063 (2007).
[31] A. M. Nemilentsau, G. Y. Slepyan, S. A. Maksimenko, A. Lakhtakia, and S. V. Rotkin, J. Nanophoton. **4**, 041865 (2010).
[32] I. V. Bondarev, G. Ya. Slepyan, and S. A. Maksimenko, Phys. Rev. Lett. **89**, 115504 (2002).
[33] I. V. Bondarev, G. Ya. Slepyan, S. A. Maksimenko, and Ph. Lambin, Carbon **42**, 997 (2004).
[34] R. Hillenbrand, F. Keilmann, P. Hanarp, D. S. Sutherland, and J. Aizpurua, Appl. Phys. Lett. **83**, 368 (2003).
[35] C. Mu, B. D. Mangum, C. Xie, and J. M. Gerton, IEEE Sel. Top. Quantum Electron. **14**, 206 (2008).
[36] D. Shi, Y. Guo, Z. Dong, J. Lian, W. Wang, G. Liu, L. Wang, and R. C. Ewing, Adv. Mater. **19**, 4033 (2007).
[37] Z. Zhou, H. G. Kang, M. L. Clarke, S. H. De Paoli Lacerda, M. Zhao, J. A. Fagan, A. Shapiro, T. Nguyen, and J. Hwang, Small **5**, 2149 (2009).
[38] W. Wang, G. Liu, H. Cho, Y. Guo, D. Shi, J. Lian, and R. Ewing, Chem. Phys. Lett. **469**, 149 (2009).
[39] L. Novotny and B. Hecht, *Principles of Nano-optics* (Cambridge University Press, Cambridge, 2006).